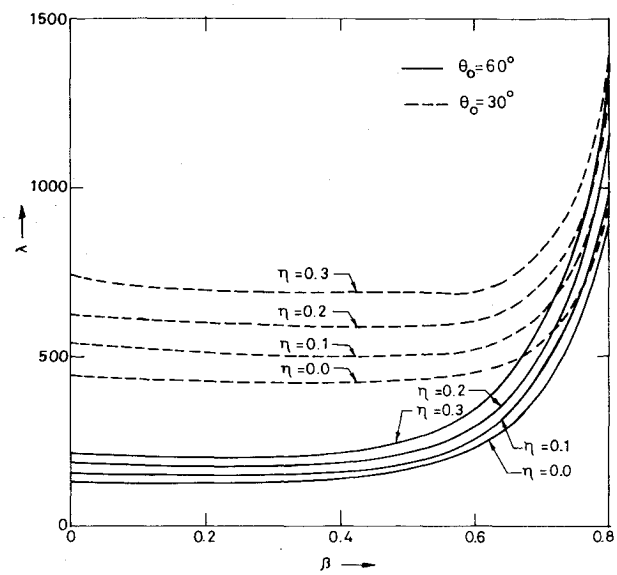

Fig. 2 Variation of stability coefficient vs radii ratio.

11×11 meshes are found to be 123.9, 122.8, 122.0, and 121.6, respectively. It is found that 9×9 mesh gives good convergence. The same mesh size has been adopted for further work and Poisson's ratio was 0.3.

Since no other results are available for comparison the annular sector plate is approximated to a square plate of constant thickness using $\theta_0 = 1.14$ deg, $b = 50.0$, and $\eta = 0$. The buckling parameter is found to be 4915, which compares well with the value of 5000 given by Levy (see Ref. 4).

A parametric study has been made varying the radii ratio β $(= b/a)$ from 0 to 0.8, the thickness parameter η from 0 to 0.3 for the sector plate angles (θ_0) of 30, 60, 90, and 120 deg. Typical results for $\theta_0 = 30$ and 60 deg are presented in Fig. 2.

It can be observed from Fig. 2 that for any annular sector plate of θ_0, if the radii ratio β is increased the critical load remains constant up to a certain value of β and then increases monotonically. It is also found that the critical load decreases as θ_0 is increased.

References

[1] Rubin, C., "Stability of Polar Orthotropic Sector Plates," *Journal of Applied Mechanics, Transactions of ASME*, Vol. 45, 1978, pp. 448-450.

[2] Srinivasan, R. S. and Ramachandran, S. V., "Stability of Clamped Skew Plates," *Journal of Structures Division, Proceedings of ASCE*, Vol. 102, 1976, pp. 569-574.

[3] Timoshenko, S. and Goodier, G. N., *Theory of Elasticity*, McGraw Hill Book Co., London, 1951.

[4] Bulson, P. S., *The Stability of Flat Plates*, Chatto and Windus Co., London, 1970.

Radiative Heat Transfer in Segregated Media

R. K. Ahluwalia* and K. H. Im*
Argonne National Laboratory, Argonne, Illinois

Nomenclature

h = enthalpy
I_b = black-body intensity
I_w = I_b at wall temperature
k_{eff} = effective thermal conductivity
n = particle size distribution function
p = pressure
Q = heat flux
R = radius
r,x = radial and axial coordinates, respectively
r_p = radius of the particle
T = temperature
u,v = axial and radial velocities, respectively
β = extinction coefficient
ϵ_w = wall emissivity
μ_{eff} = effective viscosity
ν = frequency
ρ = density
ω = scattering albedo

Introduction

THE problem of heat transfer in particle-laden flows is important in many engineering applications, such as pulverized coal combustors, oil combustors, solid propellant rocket nozzles, diffuser and radiant boilers of coal-fired magnetohydrodynamic plants, and nuclear reactors. In some of these applications a particular problem of heat transfer in a segregated medium is encountered. For instance, in a coal-burning swirl combustor the coal particles may be segregated in the core region near the injection point, and in the wall region further downstream. A question then arises as to how the stratification of a large number of absorbing (and emitting) and scattering particles influence the heat-transfer characteristics of the medium. In a previous study[1] this question was investigated by formulating a radiative heat-transfer model for a cylindrical absorbing-emitting-scattering medium, idealized to consist of two regions possessing uniform but different spectral properties. In other words, the radiation properties were assumed to suffer a step change at the interface of the two regions. An important conclusion of the study was that the segregation of particles can have a significant influence on the heat-transfer rate. A large number of particles in the highly emitting core region can enhance the heat flux inasmuch as the segregation of particles in the highly absorbing wall region can diminish the heat-transfer rate by an order of magnitude.

This Note deals with an extension of analysis conducted in Ref. 1. The restrictive assumption of the spectral properties changing discontinuously across the boundary between the two regions is relaxed. Instead, the spectral properties are considered to vary in any arbitrary and continuous fashion. In order to investigate specifically the influence of segregation of

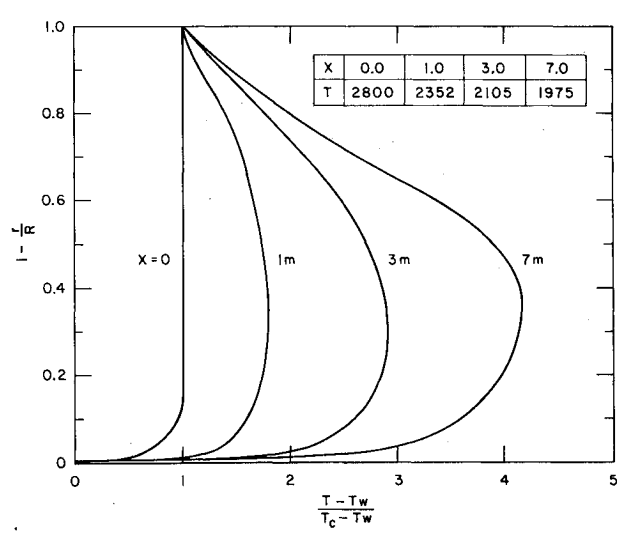

Fig. 1 Development of temperature profile with particles concentrated in the core.

Received Oct. 15, 1982; revision submitted May 20, 1983.

*Mechanical Engineer, Engineering Division.

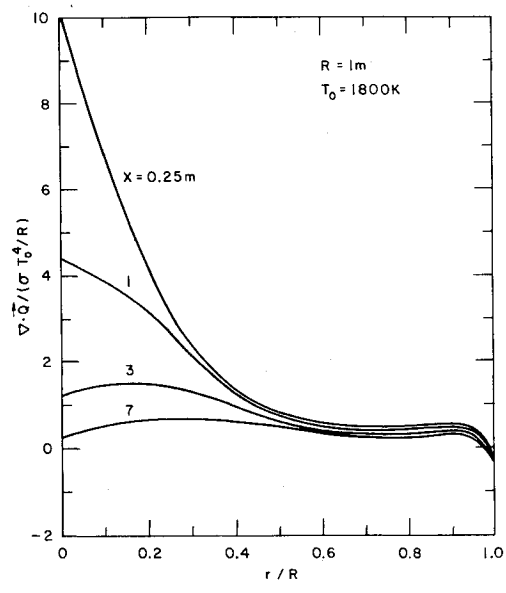

Fig. 2 Variation of divergence of radiant heat flux with particles concentrated in the core.

particles on heat transfer, a combined convection-radiation analysis is conducted in which the spectral calculations are carried out in conjunction with the determination of a temperature profile from the energy equation. The momentum and continuity equations governing the fluid motion are also solved simultaneously.

Coupled Convection and Radiation Model

Consider an axisymmetric medium that absorbs, emits, and isotropically scatters thermal radiation. Neglecting axial heat transfer and flow recirculation, the flow and thermal fields are described by the following equations:

$$\frac{\partial}{\partial x}(\rho u)+\frac{1}{r}\frac{\partial}{\partial r}(r\rho v)=0 \tag{1}$$

$$\rho u\frac{\partial u}{\partial x}+\rho v\frac{\partial u}{\partial r}=\frac{1}{r}\frac{\partial}{\partial r}\left(r\mu_{\text{eff}}\frac{\partial u}{\partial r}\right)-\frac{\mathrm{d}p}{\mathrm{d}x} \tag{2}$$

$$\rho u\frac{\partial h}{\partial x}+\rho v\frac{\partial h}{\partial r}=\frac{1}{r}\frac{\partial}{\partial r}\left(rk_{\text{eff}}\frac{\partial T}{\partial r}\right)-4\pi\int_0^\infty(1-\omega_\nu)\beta_\nu\left(I_{b\nu}-\frac{G_\nu}{4\pi}\right)\mathrm{d}\nu \tag{3}$$

The integral term in Eq. (3) is the divergence of radiant heat flux expressed in terms of the spectral incident radiation, G_ν. Application of the P_1 approximation to the radiation transport equation leads to the following equation for G_ν.

$$\frac{1}{r}\frac{\partial}{\partial r}\left(\frac{r}{\beta_\nu}\frac{\partial G_\nu}{\partial r}\right)-3(1-\omega_\nu)\beta_\nu G_\nu=-12\pi(1-\omega_\nu)\beta_\nu I_{b\nu} \tag{4}$$

For a diffusely reflecting wall, the boundary conditions for Eq. (4) are

$$\frac{\partial G_\nu}{\partial r}=0 \qquad r=0 \tag{5}$$

$$\frac{2}{3}\left(\frac{2}{\epsilon_w}-1\right)\frac{1}{\beta_\nu}\frac{\partial G_\nu}{\partial r}+G_\nu=4\pi I_{w\nu} \qquad r=R \tag{6}$$

The foregoing set of equations has been solved by a numerical technique that borrows many features from the finite difference scheme advanced by Patankar and Spalding[2] for handling parabolic flows. Some of the features included are: 1) storage of all variables except the transverse velocity v at the grid nodes, the component v being staggered in the radial direction; 2) upwind differencing for the convection terms and central differencing for the diffusion terms; and 3) determination of $\mathrm{d}p/\mathrm{d}x$ from the global continuity and the transverse velocity field from a pressure correction equation. A mixing length model is used for determining the turbulent viscosity and eddy conductivity. The radiation term in Eq. (3) is treated as a source term and evaluated for temperature distribution prevailing at the preceding step. Because of the spatial dependence of β_ν and ω_ν, Eq. (4) is solved by finite differences for G_ν. Using central differencing, the differential term in Eq. (4) is discretized as follows:

$$\frac{\partial}{\partial r}\left(\frac{1}{\beta_\nu}\frac{\partial G_\nu}{\partial r}\right)_i=\frac{1}{(r_{i+\frac{1}{2}}-r_{i-\frac{1}{2}})}\left[\left(\frac{1}{\beta_\nu}\frac{\partial G_\nu}{\partial r}\right)_{i+\frac{1}{2}}-\left(\frac{1}{\beta_\nu}\frac{\partial G_\nu}{\partial r}\right)_{i-\frac{1}{2}}\right]=\frac{1}{(r_{i+\frac{1}{2}}-r_{i-\frac{1}{2}})}\left[\frac{1}{\beta_{\nu i+\frac{1}{2}}}\frac{G_{\nu i+1}-G_{\nu i}}{r_{i+1}-r_i}-\frac{1}{\beta_{\nu i-\frac{1}{2}}}\frac{G_{\nu i}-G_{\nu i-1}}{r_i-r_{i-1}}\right] \tag{7}$$

where the subscript i denotes the grid point. The finite difference equation is written for every grid point in the radiation field, and the resulting coefficient matrix, tridiagonal in form, is easily inverted by the Gauss elimination technique.

The spectral integration in Eq. (3) is accomplished by dividing the integration domain (200-15,000 cm^{-1}) into seven bands. Integration over those bands is carried out by employing a 16-point Gaussian scheme.[1] The spectral absorption coefficients of the gaseous participating species are determined from a band model that includes the pressure broadening effect.[1] All five vibration-rotation bands of carbon dioxide and four of water vapor are considered. For particles, the efficiency factors for absorption and scattering of radiation are computed directly from the Mie theory.

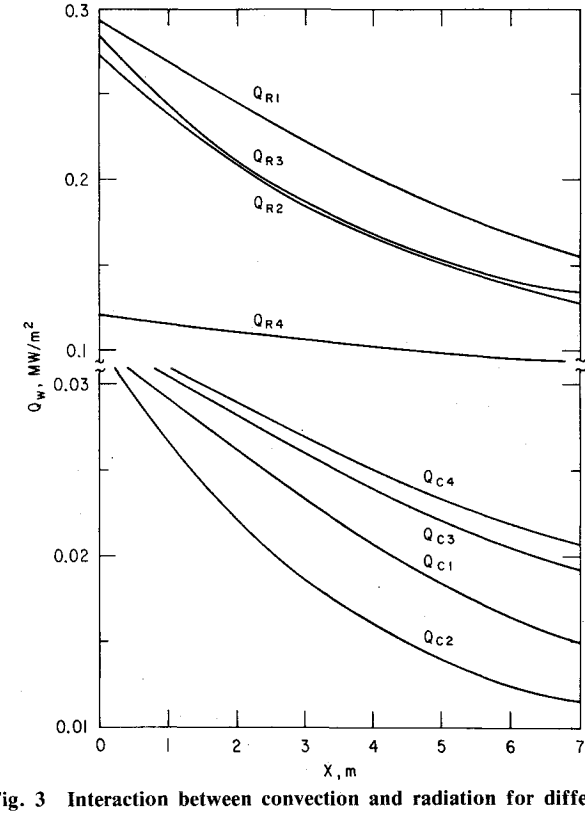

Fig. 3 Interaction between convection and radiation for different cases.

Results and Discussion

For the purpose of calculations, the particle size spectrum is assigned a fifth-order Nukiyama-Tamasawa distribution

function, and the radial distribution of the particle number density is assumed to be exponential.

$$\frac{n(r_p,r)}{N_0} = \frac{130}{\langle r_p \rangle}\left(\frac{r_p}{\langle r_p \rangle}\right)^4 \exp\left(-5\frac{r_p}{\langle r_p \rangle}\right)\exp\left(\alpha_1 \frac{r}{R}\right)$$

where α_1 is an arbitrary constant which serves to define the spatial segregation of particles, and N_0 is the particle number density at the centerline, to be determined from the particle mass flow rate.

$$\dot{m}_p = \int_0^R \int_0^\infty \frac{4}{3}\pi r_p^3 n(r_p,r)\rho_p u 2\pi r dr_p dr$$

In the foregoing equation, $\langle r_p \rangle$ is the average particle size, ρ_p is the particle mass density, and the particles have been assumed to be in velocity equilibrium with the gas. For the calculations to be presented, the following data are used: $\langle r_p \rangle = 30$ μm, $\rho_p = 2500$ kg/m^3, and $\dot{m}_p = 3$ kg/s. Additional data used are: gas flow rate = 20 kg/s, centerline gas temperature at inlet = 2800 K, wall temperature = 1800 K, channel radius = 1 m, and momentum and thermal boundary-layer thicknesses at inlet = 0.40 m. The temperature and velocity in the boundary layer at the inlet are assigned one-fifth power law profiles. For radiation calculations, the mole fractions of carbon dioxide and water vapor are taken as 0.10 and 0.15, respectively, and the wall emissivity as 0.70. The data of Foster and Howarth,[3] valid for coal particles, are used to determine the complex refractive index of particles.[1]

Three types of cases have been studied. In case 1 the particles are uniformly distributed in the flowfield ($\alpha_1 = 0$). In case 2, particles are concentrated in the wall region; here $\alpha_1 = 7$, which makes the particle number density at the wall 1100 times greater than at the centerline. In case 3, particles are segregated in the core of the flow. This situation is simulated by assigning α_1 a value of -7, so that in contrast to case 2 the particle number density at the centerline is 1100 times greater than at the wall.

For the situation of uniform distribution of particles (case 1), the development of temperature profile is similar to the pure convection flow except that the gas cools volumetrically and not just in the thermal boundary layer. Therefore, away from the wall, the temperature gradients are not as steep as in the convection-only case.

The development of temperature profile for case 2, wherein particles are segregated in the wall region, shows a significant departure from the convection-only case. In fact, at the downstream end the temperature profile resembles the parabolic laminar shape. Close to the wall, however, the temperature profile retains the sharp gradient unique to turbulent flows. Compared to the uniformly distributed particles case, the centerline temperature is much higher but the boundary layer is colder in most part.

For case 3, in which particles are concentrated in the core region, the development of temperature profile is traced in Fig. 1. A striking feature here is the shifting of the maximum temperature region from the core to an intermediate location. The evolution of this peculiar temperature profile is a direct consequence of particle concentration in the core causing an accelerated cooling of that region. As compared to the uniformly distributed particles case, the centerline temperature is much colder but the boundary layer is much hotter in most part.

The development of the temperature profiles is best understood in terms of the spatial variation of divergence of radiant heat flux. For the uniform distribution of particles (case 1), the divergence of radiant heat flux initially peaks somewhere in the boundary layer. As the temperature field develops, the peak in the boundary layer moves toward the core, weakens, and ultimately vanishes.

In case 2, the segregation of particles in the wall region leads to the appearance of a peak in the divergence of radiant heat flux in the boundary layer. Initially, this peak is nearly two times stronger than the one for the case of uniform distribution of particles. However, compared to case 1, the magnitude of divergence at the centerline is much weaker. This means that the boundary layer is being cooled much faster than in case 1 and the core much slower, thus explaining the structure of the temperature field. As the temperature field develops further, the peak moves toward the wall and relaxes in strength.

For case 3, the spatial variation of divergence of radiant heat flux at four axial locations is plotted in Fig. 2. With the particles concentrated in the core, the local absorption (and scattering) and extinction coefficients increase, as does the divergence of heat flux. Initially, the divergence of heat flux at the centerline is greater than the wall value by an order of magnitude. Consequently, the core beings to cool off very rapidly and the hottest temperature region shifts away from the core to an intermediate location (see Fig. 1). As the flow develops further, the low core temperature begins to compensate for the effect of the extinction coefficient being maximum at the centerline (due to particle concentration in the core). As a result, the magnitude of divergence of heat flux at the centerline diminishes rapidly with flow distance. Further downstream, its spatial variation is quite flat, and the maximum lies away from the centerline in spite of the particle concentration in that region. The temperature profiles of Fig. 1 are merely a reflection of the variation of divergence of radiant heat flux with radial coordinate and flow distance shown in Fig. 2.

Finally, the interaction between convection and radiation modes of heat transfer is shown in Fig. 3. In the labels of this figure, the subscript c stands for convection, R for radiation, and 1 to 3 for the three cases being considered. In addition, the results from an extra calculation are presented (subscript 4) in which only carbon dioxide and water vapor are the participating species (no particles). For uniform distribution of particles, case 1, convective and radiative heat fluxes are seen to diminish along the flow direction in an expected fashion; and radiation is the dominant mode of heat transfer. When no particles are present, case 4, the radiative heat flux drops by a factor of three (compared to case 1), indicating that particles are the major species contributing to heat transfer in case 1. Also, in the absence of particles, compared to case 1, the rate of decrease of radiative heat flux with flow distance is slower, because the temperature does not drop as rapidly; for the same reason, the convective heat flux is higher. When the particles are segregated in the wall region (case 2), the radiative heat flux diminishes in relation to that in case 1; this is attributed to the rapid cooling of the boundary layer and the low emission from the high-temperature core where fewer particles are present. The convective heat flux also decreases because of the faster growth in the thermal boundary layer. Between cases 2 and 3, the radiative flux is not substantially different because, although the particles are concentrated in the core for case 3, the large magnitude of divergence of heat flux (see Fig. 2) rapidly cools the core. Thus, in effect, after a short flow distance, the particles are trapped in a cold region, as in case 2. The key difference is that, compared to cases 1 and 2, there is an enhancement in convective heat flux due to the movement of the peak temperature region toward the wall.

References

[1] Im, K. H. and Ahluwalia, R. K., "Radiative Transfer in Spectrally-Dissimilar Absorbing-Emitting-Scattering Adjacent Mediums," *AIAA Journal*, Vol. 21, Jan. 1983, pp. 134-141.

[2] Patankar, S. V. and Spalding, D. B., "A Calculation Procedure for Three-Dimensional Parabolic Flows," *International Journal of Heat and Mass Transfer*, Vol. 15, 1972, pp. 1787-1806.

[3] Foster, P. J. and Howarth, C. R., "Optical Constants of Carbon and Coal in the Infrared," *Carbon*, Vol. 6, 1968, pp. 719-729.